Electrochimica Acta 61 (2012) 124–131

Contents lists available at SciVerse ScienceDirect

Electrochimica Acta

journal homepage: www.elsevier.com/locate/electacta

Electrochemical quartz crystal microbalance study of amorphous MnO_2 prepared by anodic deposition

Yi-Hsuan Chu [a], Chi-Chang Hu [a,*,1], Kuo-Hsin Chang [a,b,1]

[a] Department of Chemical Engineering, National Tsing Hua University, Hsin-Chu 30013, Taiwan
[b] Department of Chemical Engineering, National Chung Cheng University, Chia-Yi 621, Taiwan

ARTICLE INFO

Article history:
Received 3 September 2011
Received in revised form
21 November 2011
Accepted 25 November 2011
Available online 6 December 2011

Keywords:
a-MnO_x
EQCM
Supercapacitor
Potential window
Cycle stability

ABSTRACT

In this work, the electrochemical behavior and the corresponding mass variation of amorphous manganese oxide (denoted as *a*-MnO_x) are examined simultaneously in a neutral electrolyte containing 10 mM Na_2SO_4 without or with $NaHCO_3$ or Na_2HPO_4 by cyclic voltammetry with a quartz crystal microbalance (QCM). *a*-MnO_x was anodically deposited onto the gold-sputtered quartz electrode by means of a potentiostatic method at 1.0 V for 60 s. The morphology and microstructure of *a*-MnO_x with different potential windows of CV cycling in the above electrolyte were examined by means of the scanning electron microscopy (SEM). From this EQCM study, *a*-MnO_x is unstable between 1.0 and 1.2 V in 10 mM Na_2SO_4 because of significant dissolution of *a*-MnO_x. The repeated potential cycling promotes the electrocatalytic activity of *a*-MnO_x for oxygen evolution, which also enhances the dissolution of *a*-MnO_x. The dissolution phenomenon and oxygen evolution are successfully suppressed by the formation of insoluble manganese carbonate or the adsorption of phosphate by adding $NaHCO_3$ or Na_2HPO_4 in the Na_2SO_4 electrolyte, enlarging the potential window for the charge/discharge of *a*-MnO_x.

1. Introduction

Supercapacitors have been widely recognized as a complementary charge storage assistance to rechargeable batteries, fuel cells, wind power, and solar cells because of their high charge/discharge efficiency, high power properties, and very long cycle life [1,2]. Applications of this kind of devices become more important to the cases which require transient but high/peak power pulses of charge/discharge for time-dependent usage [3] because supercapacitors with a much lower equivalent series resistance (ESR), in comparison with rechargeable batteries, can capture and store pulse energy during the braking process, leading to a much higher energy efficiency [3,4].

In general, supercapacitors can be divided into three categories according to the charge storage mechanism of devices. The so-called electrical double layer capacitors (EDLCs) use the electrostatic charge separation at the electrolyte–electrode interface, showing the importance of increasing the electrolyte-accessible surface area [5–7]. Pseudocapacitors with a mechanism similar to rechargeable batteries employ fast superficial redox reactions [1,2,4]. In comparing with EDLCs, higher specific capacitance can be achieved by using redox-active materials and supercapacitors of the asymmetric type are developed to further enhance the energy density of devices [8]. Moreover, supercapacitors of the asymmetric type can be further divided into two forms, i.e., double-layer/redox and redox/redox types since asymmetric indicates that the active materials in the anode are different from that in the cathode. Accordingly, developing electrode materials promising to EDLCs or pseudocapacitors are equally important to the application of asymmetric type.

Crystalline ruthenium dioxide (RuO_2) in the hydrous form has been widely recognized as the best electrode materials for pseudocapacitors because of its high specific capacitance, good electronic conductivity, and cycle stability [9,10]. However, due to cost and environment considerations, other transition metal oxides, such as MnO_x [11], CoO_x [12], VO_x [13], Fe_3O_4 [14], Ni–Co oxides [15,16], and WO_3 [17] are recommended to replace RuO_2. Among these pseudocapacitor electrode materials, manganese oxides in both amorphous and crystalline forms are the most promising candidate because of their excellent reversibility and acceptable specific capacitance [11,18] although the cycle stability of MnO_x is not satisfactory [19]. Fortunately, the cycle stability of amorphous MnO_x (denoted as *a*-MnO_x) was found to be significantly improved by introducing suitable anions (e.g., $HPO_4{}^{2-}$ or $HCO_3{}^{-}$) into the electrolyte [20] or by adding Mn_3O_4 into the active material [21].

In developing pseudocapacitive materials, gaining insights on the mechanisms of charge storage and performance degradation

---

[*] Corresponding author at: Department of Chemical Engineering, National Tsing Hua University, 101, Section 2, Kuang-Fu Road, Hsin-Chu 30013, Taiwan.
Tel.: +886 3 573 6027; fax: +886 3 573 6027.
E-mail address: cchu@che.nthu.edu.tw (C.-C. Hu).
[1] ISE Member.

0013-4686/$ – see front matter © 2011 Elsevier Ltd. All rights reserved.
doi:10.1016/j.electacta.2011.11.106

is of both academic and practical interests. For example, Na^+ and H_3O^+ cations from aqueous electrolytes were proposed to involve in the charge storage process of MnO_x, evidenced by X-ray photoelectron spectroscopic (XPS) [18] and electrochemical quartz crystal microbalance (EQCM) [22] analyses. Moreover, $HPO_4{}^{2-}$ and $HCO_3{}^-$ were proposed to reduce the dissolution of Mn^{2+} by forming indissoluble Mn^{2+} salts [20]. However, the potential region responsible for the formation of Mn^{2+} and the deposition rate of the indissoluble Mn^{2+} salts are important to improve the oxide degradation issue. In this work, the voltammetric and quartz crystal microbalance responses were employed to gain the degradation information of a-MnO_x in neutral aqueous media. The introduction of $HPO_4{}^{2-}$ and $HCO_3{}^-$ on the formation of indissoluble Mn^{2+} salts and the improvement of a-MnO_x cycle stability was also investigated.

2. Experimental

Amorphous MnO_x was deposited onto an Au/Ti-sputtered quartz crystal working electrode in the EQCM cell under the potentiostatic mode at 1.0 V for 1 min. The size of the whole EQCM electrode is 0.205 cm^2. The diameter of the quartz crystal is 13.7 mm. The diameter of the gold electrode for a-MnO_x deposition is 5.11 mm. The reference crystal has an oscillation frequency of 8.000 MHz and the working crystal oscillation frequency is between 7.995 and 7.950 MHz. The mass of a-MnO_x was simultaneously monitored by the quartz crystal microbalance. After deposition, the electrode was washed with deionized water several times and dried in an oven at 85 °C overnight. The deposition bath contained 5 mM $Mn(CH_3COO)_2{\cdot}4H_2O$ (Showa EP, Japan). All solutions used in this work were prepared with deionized water produced by a reagent water system (Milli-Q SP, Japan) at 18 MΩ cm. All reagents, not specified, without further purification are Merck, GR. Solution temperature was maintained at room temperature (under an air condition at 25 °C).

Cyclic voltammetric (CV) and EQCM responses were conducted by an electrochemical analyzer (CHI4051a, CH Instruments Inc.) in a solution containing 10 mM Na_2SO_4 with/without Na_2HPO_4 (J.T. Baker AR, USA) or $NaHCO_3$ (Hanawa EP, Japan). The reference and counter electrodes were Ag/AgCl (Argenthal, 3 M KCl, 0.207 V vs. SHE at 25 °C) and a platinum wire (99.95%, 0.5 mm in diameter and 5 cm in length), respectively. The surface morphologies of a-MnO_x before and after CV cycling were examined by a field-emission scanning electron microscope (FE-SEM, Hitachi S4800-type I).

3. Results and discussion

3.1. EQCM and morphology studies of as-deposited a-MnO_x

Fig. 1 shows the typical current–time and mass–time curves during the electrodeposition process of a-MnO_x. In Fig. 1a, upon imposing the potential at 1.0 V, the deposition current rises to a high value due to the double-layer charging effect and the extremely high concentration gradient of Mn^{2+} at the electrode–electrolyte interface since Mn^{2+} at the electrode surface must be effectively consumed and the concentration of Mn^{2+} decreases immediately to 0 when the electrode potential is stepped to 1.0 V. The later statement is supported by the fact that the applied overpotential for depositing a-MnO_x in this work is about 0.6 V because the onset deposition of a-MnO_x from $Mn(CH_3COO)_2{\cdot}4H_2O$ was found to be 0.4 V and the deposition process was under diffusion control at potentials positive than ca. 0.75 V [23]. The gradual decrease in current to 46 μA with prolonging the deposition time to 60 s is attributed to the continuous decrease in the concentration gradient of Mn^{2+} at the electrode–electrolyte interface with the deposition time [11]. On curve 2 of Fig. 1b, the mass of a-MnO_x initially increases at a high rate and then, increases linearly with deposition time beyond 13 s. In order to correlate the deposition current and the deposition rate, the first derivative of mass–time curve is added as curve 1 in Fig. 1b. From a comparison of Fig. 1a and curve 1 in Fig. 1b, the rate of a-MnO_x deposition and the current–time curve are very similar. Hence, the current efficiency of a-MnO_x deposition is expected to be high. This speculation is also supported by the result that the mass of a-MnO_x has been found to be directly proportional to the passed charge [24]. Based on the Faraday law, the theoretical mean deposition rate of a-MnO_x is 50 ng/s when the total charge of this 60-s deposition process is 4 mC and $m/n = 0.35$.

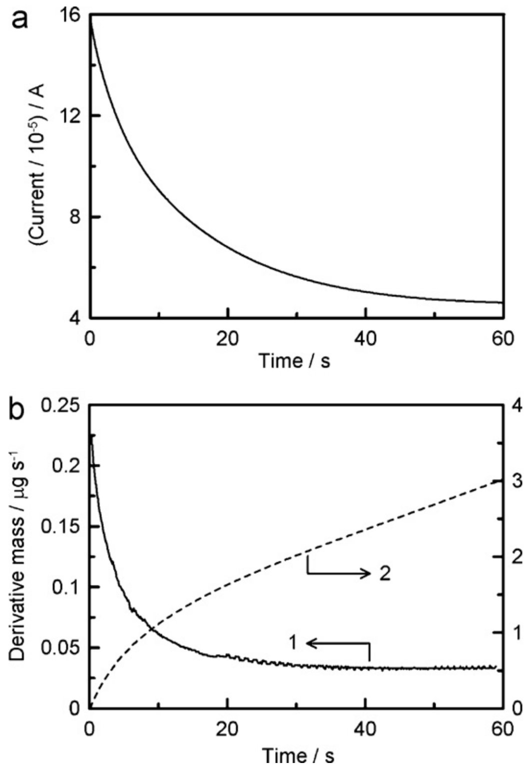

Fig. 1. (a) Current–time curve of a-MnO_x deposited at 1.0 V for 1 min from a solution containing 5 mM $Mn(AcO)_2{\cdot}4H_2O$. (b) The corresponding (1) first derivative of mass–time curve and (2) mass–time curve for the deposition of a-MnO_x.

$$(n+m)Mn^{2+} + 2(n+m)H_2O \rightarrow (MnO_2)_n(MnOOH)_m + (4n+3m)H^+ + (2n+m)e \quad (1)$$

This result indicates that the mean oxidation state of a-MnO_x is 3.74. However, due to the hydrous nature of as-deposited a-MnO_x, the amount of Mn species in the deposit should be lower. Accordingly, the mean oxidation state of a-MnO_x should be lower than 3.74, which was reported to be 3.43 [25].

Fig. 2a and b shows the SEM images of a bare EQCM electrode and that deposited with a-MnO_x, respectively. Clearly, the morphology of sputtered Au/Ti is relatively dense and compact with clear grain boundaries. The as-deposited a-MnO_x is a highly porous film with a uniform nanostructure of a three-dimensional (3D) network. In addition, no obvious grain boundaries can be found on this deposit and several pores are covered with sheet-like a-MnO_x films. The mean diameter of these MnO_x nanowires is about 10 nm meanwhile the diameter of pores is about 30–50 nm, favorable for the electrolyte penetration during the charge/discharge process for the supercapacitor application. The morphology of this as-deposited a-MnO_x film resembles that prepared by cyclic voltammetry between 0.4 and 1.0 V for 30 cycles in our previous work [25], which generally showed a higher specific capacitance.